

中国激光

国产 Invar 合金激光焊接接头组织演变及拉伸性能研究

周裕琦¹, 程立宏¹, 王建峰¹, 李柱², 穆战², 占小红^{1*}

¹南京航空航天大学材料科学与技术学院, 江苏 南京 211106;

²西安钢研功能材料股份有限公司, 陕西 西安 710000

摘要 针对 4 mm 厚的国产 Invar 合金进行激光焊接实验, 对比分析了不同热输入下接头显微组织的差异性, 并探究了晶粒尺寸对接头拉伸性能的影响。结果表明, 焊缝区域主要由柱状晶组成, 在不同热输入下晶粒的生长模式几乎相似, 但柱状晶晶粒的尺寸随着热输入的增加而逐渐增大。低热输入(90 J/mm)条件下的平均晶粒面积为 $12599.7 \mu\text{m}^2$, 比高热输入(200 J/mm)条件下的细化了 29.8%。相比于高热输入, 低热输入时焊缝底部的亚晶粒数量增多且尺寸减小, 平均二次枝晶间距从 6.11 μm 左右下降到 4.26 μm 左右。拉伸结果表明, 热输入增加引起的晶粒粗化导致接头的抗拉强度由 473.4 MPa 下降至 432.9 MPa, 同时断口处等轴韧窝的尺寸和深度明显减小。

关键词 激光技术; 激光焊接; 国产 Invar 合金; 组织演变; 晶粒尺寸; 拉伸性能

中图分类号 TG456.7 文献标志码 A

DOI: 10.3788/CJL230861

1 引言

Invar 合金自 19 世纪被科学家发现以来, 以其极低的热膨胀系数而一直备受重视^[1-3]。Invar 合金具有与复合材料极为相近的热膨胀系数, 因此被广泛用作航空航天领域大型复材模具结构的重要材料^[4-5]。然而, 由于材料的特殊性, 其生产技术壁垒高, 特别是在高端领域的应用难度较大, 而其生产技术一直被国外垄断, 故 Invar 合金的国产化具有重要意义。

目前, 国内仅有少数企业实现了小批量 Invar 合金的国产化生产, 而在 Invar 合金的国产化研制过程中, 其热物理性能和力学性能是主要关注的内容。在 Invar 合金的制造方面: Wang 等^[6]通过添加富含 Zr 的金属间化合物, 有效降低了 Invar 合金的热膨胀系数; Jiao 等^[7]指出, 沉淀相(Nb, C)是电弧增材制造 Invar 合金的热膨胀系数降低和性能提高的原因; Rao 等^[8]研究了 Fe₆₆Ni₂₉Co₅ 合金中奥氏体相在冷却过程中的转变行为和晶格畸变, 认为晶格畸变的演化对于 Invar 效应是至关重要的。在 Invar 合金的激光焊接研究中: 吴东江等^[9-10]探究了 Invar 合金薄板的脉冲激光焊接工艺, 发现激光功率和脉宽是影响焊缝熔深、熔宽和热影响区大小的主要因素; Li 等^[11]研究了 5 mm 厚 Invar 合金激光焊接接头的热膨胀系数和拉伸性能, 发现焊缝的热膨胀系数和居里温度与母材几乎相同, 但接头的拉伸强度仅为母材的 69.2%; Zhao 等^[12]通过模拟激光摆动焊接过程中的熔池流动行为, 发现光束摆动引起的涡

采用光纤激光器作为本次实验的激光光源, 其最

流对熔池具有搅拌作用, 有助于细化焊缝晶粒并提高拉伸性能; Li 等^[13]研究了表面粗糙度对 Invar 合金焊接接头力学性能的影响, 通过增加表面粗糙度, 可提高激光功率的吸收率, 进而显著改善焊缝熔深, 但会出现晶粒粗大和接头软化的现象。综合国内外研究现状可知, 目前针对 Invar 合金的研究主要是关注引起热膨胀效应变化的因素和微观组织对力学性能的影响两个方面, 而有关焊接热输入对 Invar 合金激光焊接接头组织演变和拉伸性能的影响的研究还较少, 所以有必要开展热输入对国产 Invar 合金组织演变和拉伸性能的影响的研究, 掌握相关机理规律, 为国产 Invar 合金的应用及推广提供支持。

本文采用三种不同热输入的工艺参数对 4 mm 厚的国产 Invar 合金板材进行激光焊接实验, 焊后对比分析了热输入对接头微观组织的影响, 并探究了焊缝区域的晶粒形态和晶粒尺寸对接头拉伸性能的影响。

2 实验材料与方法

本实验选用西安钢研功能材料股份有限公司自研生产的国产 Invar 合金(退火态)作为焊接母材, 其化学成分如表 1 所示。将国产 Invar 合金板材切割成尺寸为 100 mm × 50 mm × 4 mm 的焊接试板, 其三维几何结构如图 1 所示。Invar 合金试板表面易被氧化, 形成的氧化膜影响接头的焊接质量, 因此焊接前使用角磨机对试板待焊区域的上表面、侧壁和下表面等区域进行彻底打磨, 然后用化学方法严格清洗表面的油污。大输出功率为 6 kW, 输出激光波长为 1080 nm, 激光束

收稿日期: 2023-05-25; 修回日期: 2023-06-18; 录用日期: 2023-07-11; 网络首发日期: 2023-07-19

通信作者: *xiaohongzhan_nuaa@126.com

表 1 国产 Invar 合金的化学成分
Table 1 Chemical compositions of domestic Invar alloy

Element	Ni	Mn	Si	Al	Ti	C	Fe
Mass fraction /%	36.040	0.350	0.180	0.047	0.066	0.023	Bal.

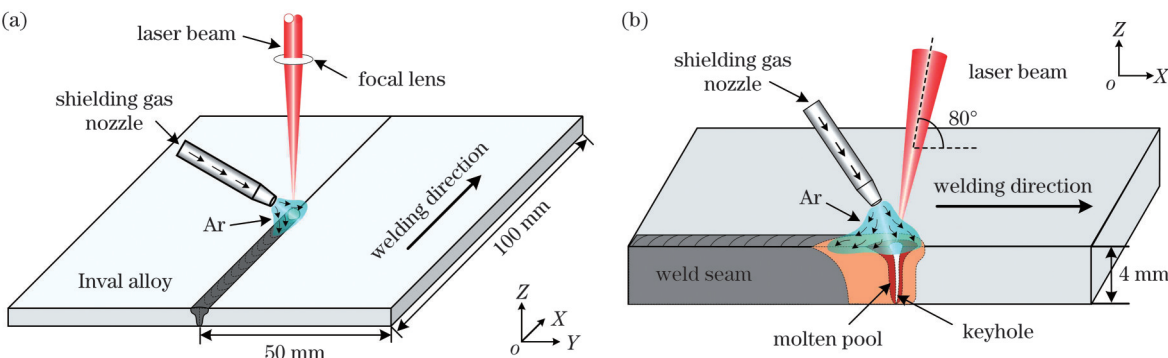


图 1 激光焊接示意图。(a)激光焊接;(b)熔池形貌

Fig. 1 Schematics of laser welding. (a) Laser welding; (b) molten pool morphology

经过准直镜与聚焦镜后作用在板材表面,激光光斑直径为 0.1 mm。由于 Invar 合金的 Ni 含量较高且导热系数较低,液态熔池的流动性较差,熔池在高温下的停留时间长^[14],故为了保护熔池不被氧化,采用纯度(体积分数)为 99.99% 的氩气作为保护气体,气体流量为 20 L/min,采用三组热输入不同的焊接工艺参数(表 2)对试板进行激光焊接。

焊接结束后通过观察测试焊接接头的微观组织和拉伸性能,分析热输入对国产 Invar 合金激光焊接接头显微组织的影响,并探究晶粒尺寸对接头拉伸性能的影响。截取焊缝表面形貌良好的区域制备金相试样,对金相试样进行研磨、抛光,使用硝酸乙醇进行腐蚀,采用光学显微镜对焊缝的几何形状与微观组织形态进

表 2 国产 Invar 合金的激光焊接工艺参数

Table 2 Laser welding process parameters of domestic Invar alloy

No.	Laser power P / (W)	Welding speed v / (m·min ⁻¹)	Heat input / (J·mm ⁻¹)
1	2250	1.5	90
2	3000	1.5	150
3	3000	1.2	200

行观察分析,采用电子背散射衍射(EBSD)技术对焊缝晶粒尺寸及晶粒取向进行观察。拉伸试样保留焊缝余高,采用电子万能拉伸试验机测试了焊缝试样的室温拉伸性能,并采用扫描电子显微镜(SEM)对断口形貌进行了观察。测试试样的取样位置及拉伸试样的尺寸示意图如图 2 所示。

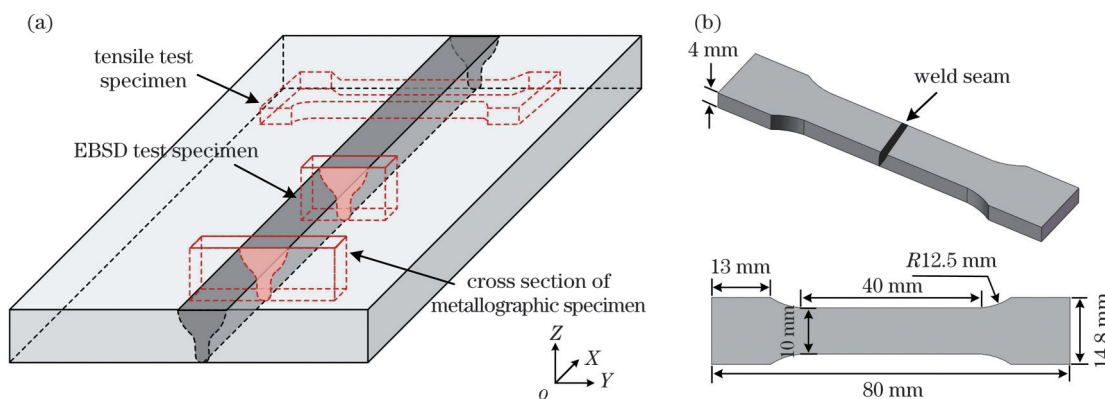


图 2 试样取样位置及尺寸示意图。(a)取样位置;(b)拉伸试样尺寸

Fig. 2 Schematics of sampling position and size of specimen. (a) Sampling position; (b) size of tensile specimen

3 分析与讨论

3.1 焊接接头的宏观形貌

图 3 为不同热输入下焊缝的横截面形貌和宏观形貌。由图 3 可知,材料在焊接过程中受到激光热量的作用而产生不同的相变行为,焊接接头不同区域的组

织差异较为明显。因此激光焊接接头可以分为三个区域:焊缝熔化区、母材区和较窄的热影响区,在焊缝中心处有明显的晶粒生长交汇的界线。在低热输入(90 J/mm)条件下,焊缝横截面呈现高脚杯状,焊缝上表面的鱼鳞纹分布较为均匀,并且飞溅很少。随着热输入增加到 150 J/mm,即激光功率提高至 3000 W,熔

池中的 Marangoni 对流导致焊缝横截面呈现 X 形状, 其上表面鱼鳞纹的分布逐渐不均匀, 且产生较多的飞溅。当热输入增加至 200 J/mm, 即焊接速度降低至

1.2 m/min 时, 焊缝上表面的鱼鳞纹分布相较于热输入 150 J/mm 时较为均匀, 且产生的飞溅减小; 此外, 焊缝横截面的尺寸明显比其他热输入时大。

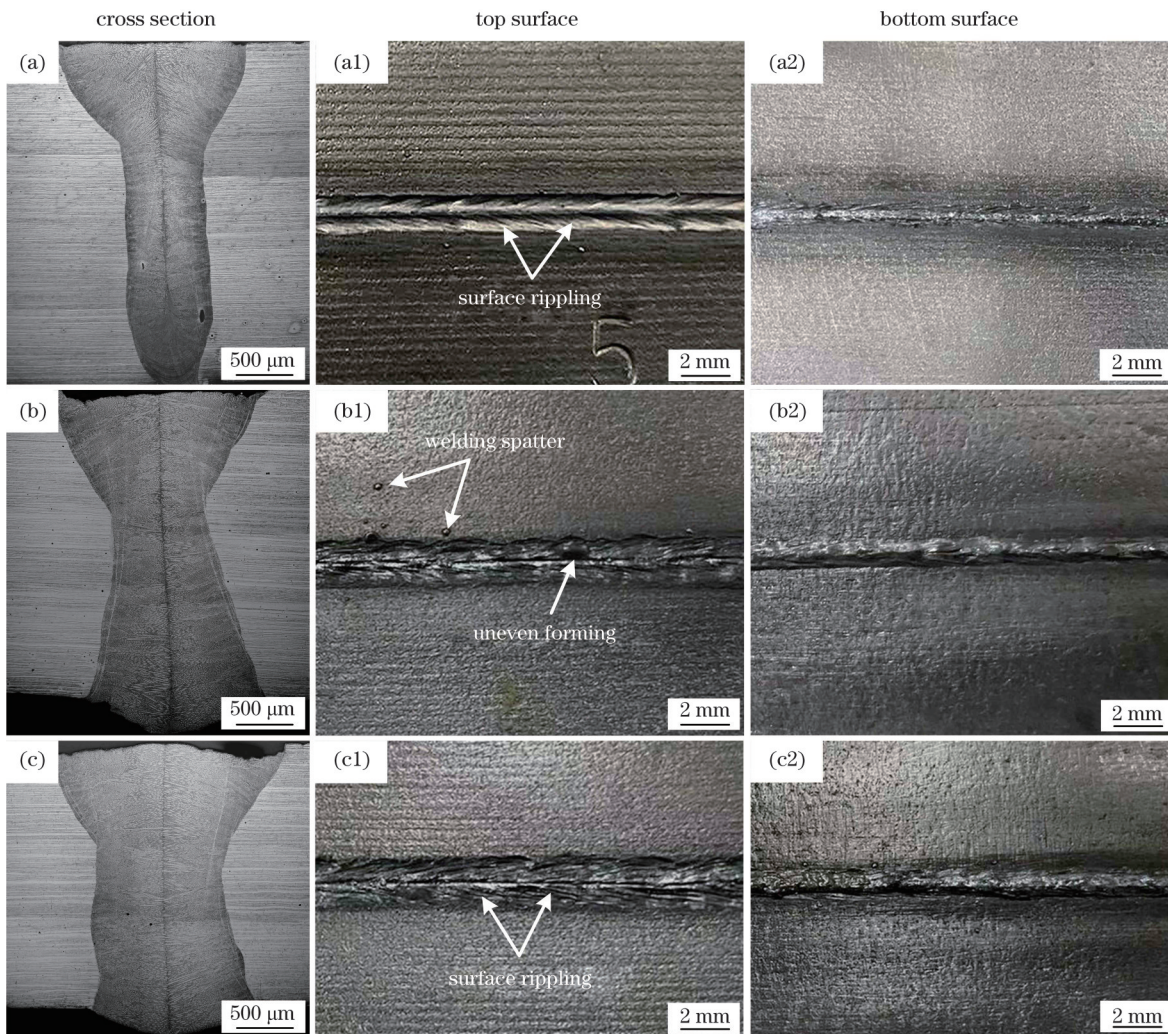


图3 不同热输入下的焊缝形貌。(a)(a1)(a2)低热输入(90 J/mm);(b)(b1)(b2)中热输入(150 J/mm);(c)(c1)(c2)高热输入(200 J/mm)

Fig. 3 Weld morphologies under different heat inputs. (a)(a1)(a2) Low heat input (90 J/mm); (b)(b1)(b2) medium heat input (150 J/mm); (c)(c1)(c2) high heat input (200 J/mm)

为了定量研究热输入对熔池尺寸的影响, 对熔池大小的相关特征进行了定量分析, 结果如图 4 所示。可以看出: 随着焊接热输入的增加, 焊缝的上表面熔宽(W_u)、焊缝中部熔宽(W_m)和焊缝下部熔宽(W_l)逐渐增加, 高热输入下的焊缝上表面熔宽约为 2.67 mm, 低热输入下的焊缝上表面熔宽约为 2.23 mm; 激光功率的增加导致焊缝下部熔宽的增加相对较为明显, 焊接速度的降低导致焊缝上表面熔宽和焊缝中部熔宽的增加相对较为明显; 而随着焊接热输入的增加, 焊缝上部的高度呈现先上升后下降的趋势, 在热输入为 150 J/mm 时达到最高值, 约为 1.31 mm。

3.2 焊接接头的微观组织

图 5 为不同热输入下的微观组织, 可以看出: 由于

激光热源能量集中且加热范围小, 焊接接头的热影响区(HAZ)较窄, 并且在焊接热循环的作用下, HAZ 中的晶粒比母材粗大; 焊缝(WS)区域以较大的柱状晶粒为主, 并且在不同的热输入下晶粒的生长模式几乎相似; 上部区域的晶粒向上生长, 中部区域的晶粒对向生长, 而下部区域的晶粒的生长方向偏向于下部, 但均垂直于熔合线。在低热输入(90 J/mm)条件下, 熔池的温度梯度大, 冷却速度快, 柱状晶粒的生长受限, 晶粒尺寸相对较小^[15]; 随着焊接热输入的增大, 液态熔池经历的最高温度逐渐增加, 容易导致晶界的迁移和晶粒的粗化; 同时由于 Invar 合金的晶界迁移激活能较低, 在熔池固液界面处液相凝固时晶粒形核形成新相所需的能量较小^[16], 故焊缝区域的柱状晶晶粒尺寸随着热输入的增加而逐渐增大。图 5 还显示了焊缝熔合线与

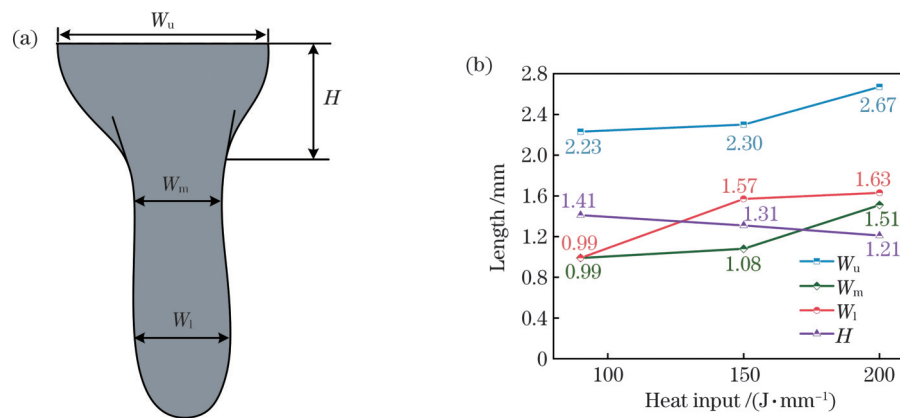


图 4 热输入对熔池尺寸的影响。(a)典型熔池示意图;(b)不同热输入下的相应尺寸

Fig. 4 Effect of heat input on molten pool dimension. (a) Schematic of typical molten pool; (b) corresponding dimensions under different heat inputs

中心线之间及焊缝中心的亚晶粒组织形态,焊缝由各种尺寸的柱状枝晶和等轴枝晶组成,柱状枝晶分布在不同方向上;在焊缝中心线附近能观察到清晰的一次

枝晶和二次枝晶,并且随着热输入的增加,焊缝中心线附近出现了少量的细小等轴亚晶结构。

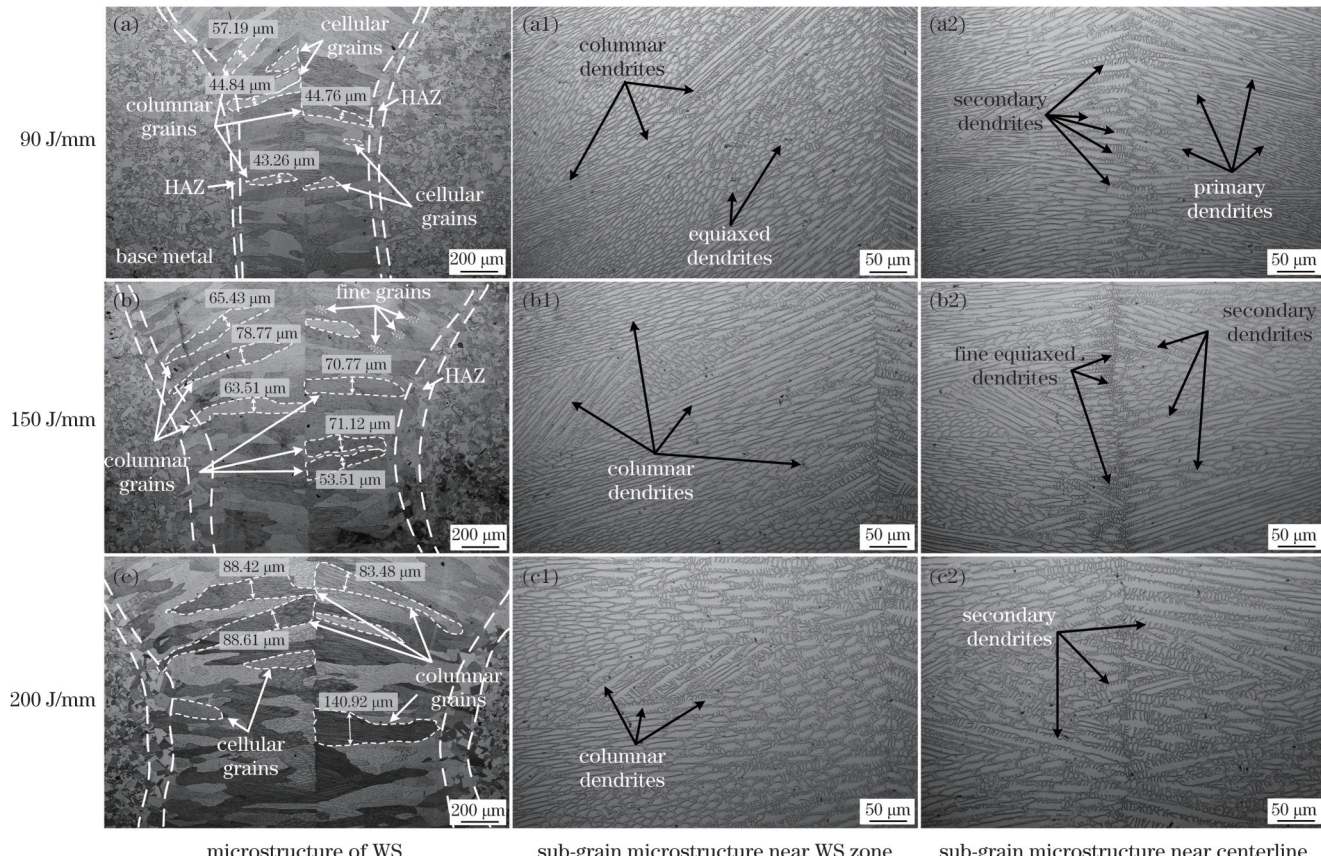


图 5 不同热输入下的微观组织形貌

Fig. 5 Microstructures under different heat inputs

Invar 合金中的 Ni 含量较高,且是合金含量较高的单相奥氏体合金,同时由于液相在熔池固液界面处母材奥氏体晶粒表面上形核形成新相时,结晶点阵形式及点阵常数均与新相相似,故界面张力小,有利于新相形核,这使得激光焊接熔池边缘的晶粒呈现出典型的外延生长形貌;加之高速焊接,使得 Invar 合金激光焊

接头的金属凝固过程是一个以母材为基底外延生长的快速、定向凝固过程,熔池中晶粒的生长方向均垂直于熔合线。图 6 显示了熔池凝固过程中组织的生长条件。由基于固液界面稳定性的成分过冷理论^[17]可知,当达到成分过冷条件时,在凝固前沿形成固液两相区,该区域将发生自发结晶形核、晶粒生长和枝晶演化等

过程,其温度梯度(G)与冷却速度(R)之比决定的成分过冷度对凝固组织枝晶形态的影响较大。在靠近母材的熔池边缘,温度梯度高,成分过冷度小,组织以胞状晶形态生长;随着凝固的进行,温度梯度逐渐减小,冷却速度逐渐增加,成分过冷区逐渐增大,组织形态由胞

状晶向树枝晶转变,并促进了二次枝晶的生长;随着温度梯度的进一步减小并逐渐趋于稳定,熔融金属将同时过冷,此时在焊缝中心处产生新的等轴枝晶,而定向树枝晶的生长受阻,导致柱状枝晶向等轴枝晶转变,最终形成图 6(d)所示的晶粒分布形态。

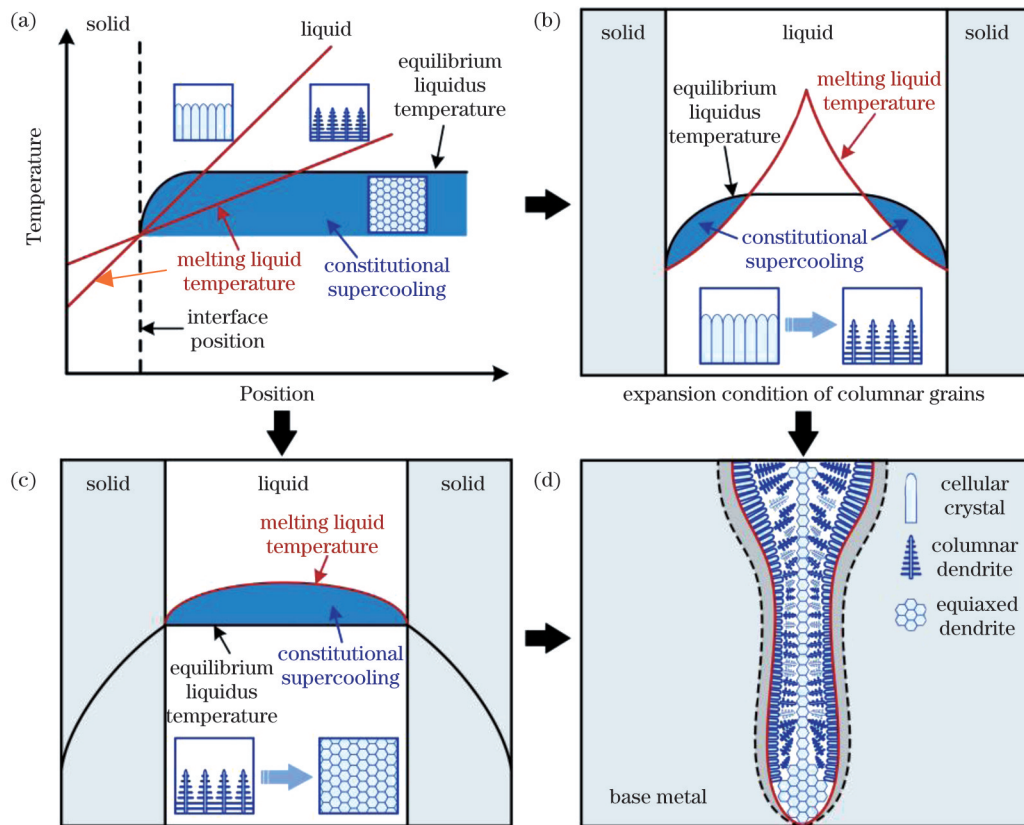


图 6 熔池凝固过程中组织生长条件示意图。(a)成分过冷条件;(b)柱状晶的扩展阶段;(c)等轴晶的形成阶段;(d)焊缝晶粒分布
Fig. 6 Schematics of microstructure growth conditions during molten pool solidification process. (a) Constitutional supercooling condition; (b) expansion stage of columnar grains; (c) formation stage of equiaxed grains; (d) weld grain distribution

3.3 焊接接头的晶粒尺寸

采用 EBSD 分析低热输入(90 J/mm)和高热输入(200 J/mm)下焊缝的晶粒形态和晶粒尺寸,图 7 为不同热输入下的反极图(IPF)、极图(PF)、晶粒尺寸和晶粒取向差分布直方图。由图 7(a)、(b)可知,焊缝的晶粒是垂直熔合线并沿热流方向定向凝固生长的柱状晶形态,在高热输入条件下,焊缝中部的晶粒取向较为杂乱,呈现一定的等轴晶粒特征,且晶粒尺寸较为粗大,而低热输入时焊缝中部的晶粒尺寸较为细小。从极图可以看出,在焊接过程中面心立方(FCC)结构的晶粒最容易沿着 $<001>$ 生长,生长最快的晶粒将取代非优先取向的晶粒,且高热输入下的晶粒竞争生长机制比低热输入下的强烈。由于有大量的柱状晶粒,故采用统计晶粒面积的方式进行比较^[18],高热输入(200 J/mm)条件下的平均晶粒面积为 $17956.6 \mu\text{m}^2$,而低热输入(90 J/mm)条件下的平均晶粒面积为 $12599.7 \mu\text{m}^2$,后者比前者细化了 29.8%。对于多晶材料,取向差角度小于 10° 的晶界为小角度晶界,而大于 10° 的晶界为高

角度晶界。高角度晶界会阻碍脆性裂纹的扩展,增加其比例和数量有利于提高焊接性能^[19]。两种热输入下的晶粒主要为小角度取向差,但低热输入(90 J/mm)下大角度取向差的含量比高热输入(200 J/mm)下的高^[20]。

图 8 为焊缝底部的等轴亚晶粒结构与焊缝中心线附近的二次枝晶,采用边长为 $20 \mu\text{m}$ 的正方形定量分析焊缝底部亚晶粒的尺寸^[21]。当热输入为 90 J/mm 时,亚晶粒数量(N)较多,尺寸相对较小,当热输入增加至 200 J/mm 时,亚晶粒的数量明显减小,这意味着晶粒尺寸相对较大。根据一定长度上二次枝晶壁的数目计算二次枝晶间距并求平均值^[22],其中 L1、L2 和 L3 为二次枝晶晶粒截取位置和范围。在低热输入(90 J/mm)时,测量得到的平均二次枝晶间距约为 $4.26 \mu\text{m}$,当热输入增加到 150 J/mm 时,平均二次枝晶间距增加到 $5.12 \mu\text{m}$ 左右,而在高热输入(200 J/mm)下,平均二次枝晶间距约为 $6.11 \mu\text{m}$ 。正如 Ren 等^[23]指出的,二次枝晶间距主要与冷却速度有关,冷却速度越

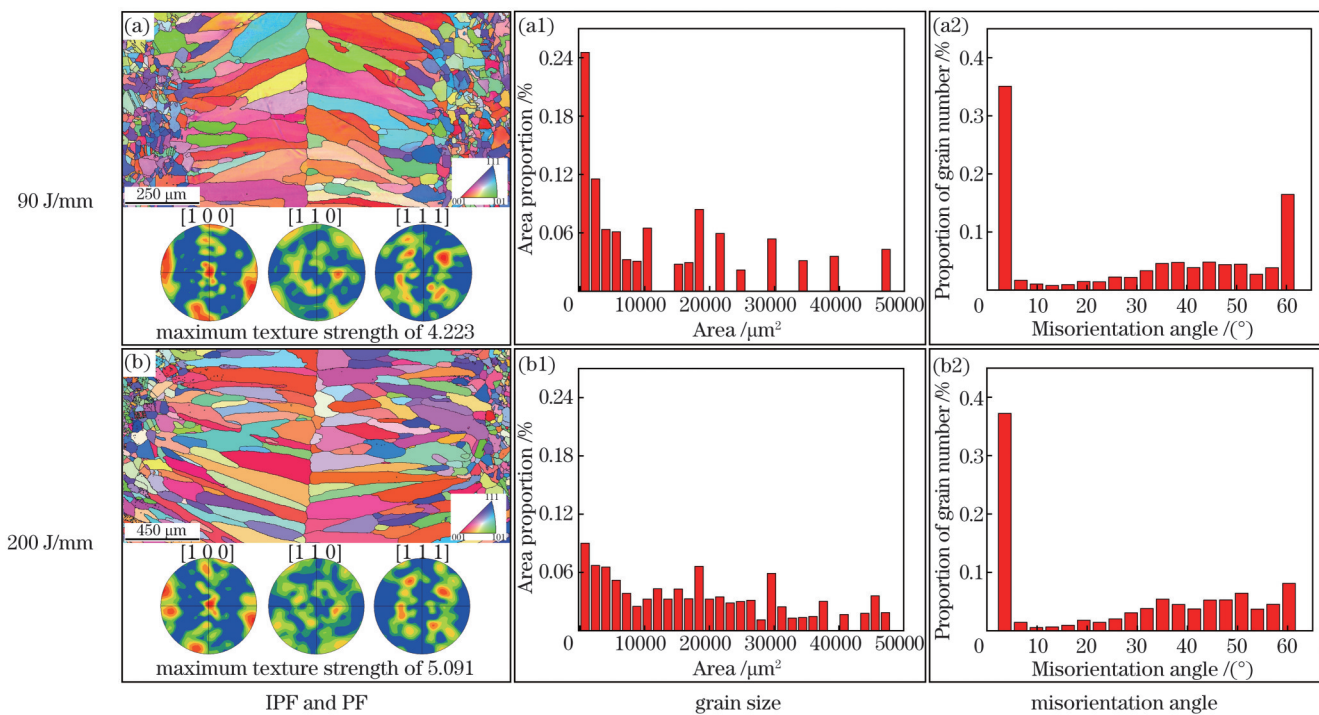


图 7 不同热输入下的 IPF 图、极图、晶粒尺寸和晶粒取向差分布直方图

Fig. 7 IPFs, PFs, and distribution histograms of grain sizes and misorientation angles under different heat inputs

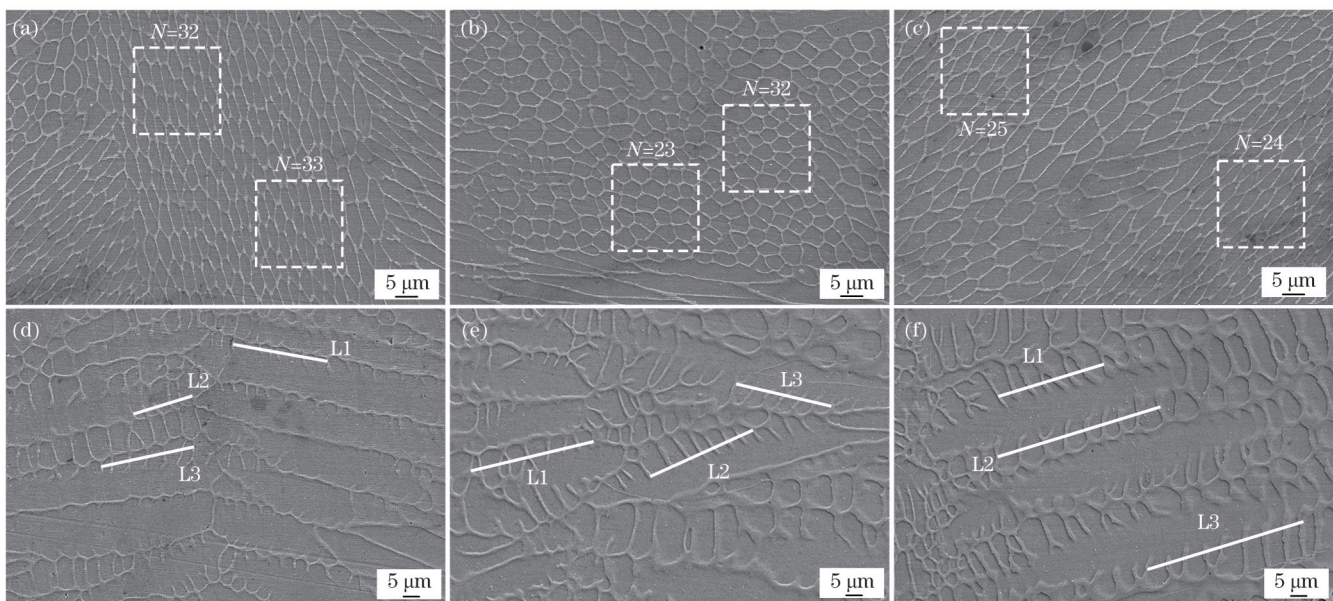


图 8 不同热输入下焊缝底部的亚晶粒结构与焊缝中心线处的二次枝晶。(a)(d)低热输入(90 J/mm);(b)(e)中热输入(150 J/mm);(c)(f)高热输入(200 J/mm)

Fig. 8 Sub-grain structures at WS bottom and secondary dendrites at centerline of WS under different heat inputs. (a)(d) Low heat input (90 J/mm); (b)(e) medium heat input (150 J/mm); (c)(f) high heat input (200 J/mm)

快, 二次枝晶间距越小。

3.4 晶粒尺寸对拉伸性能的影响

对三种热输入下的国产 Invar 合金激光焊接接头进行拉伸实验, 其结果如图 9 所示。可以看出, 三种热输入下接头的抗拉强度分别是 473.4、446.2、432.9 MPa, 其断裂位置均位于焊缝区域。随着热输入的增加, 接头的抗拉强度逐渐降低, 延伸率从 20.7% 下降至 15.3%, 说明晶粒的形态和尺寸会影响焊接接头局部

区域的应力-应变分布, 从而影响接头的强度和塑性; 而低热输入下焊缝中晶粒的高角度晶界比例和数量比高热输入下的大, 因此相比之下其抗拉强度最优; 此外, 晶粒尺寸大的区域易在外力作用下产生位错滑移, 因此更容易断裂。

图 10 为接头拉伸断口的扫描电镜(SEM)照片, 可以发现, 国产 Invar 合金激光焊接接头的断裂机制为塑性断裂, 在断裂处能观察到许多等轴韧窝, 表明接头的

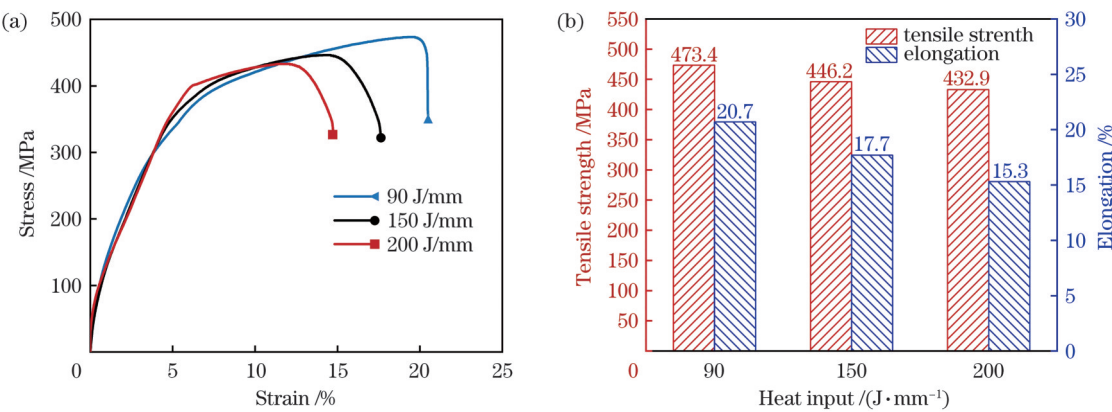


图 9 不同热输入下焊缝的拉伸测试结果。(a)应力-应变曲线;(b)抗拉强度与伸长率

Fig. 9 Tensile test results of weld seam under different heat inputs. (a) Stress-strain curves; (b) tensile strength and elongation

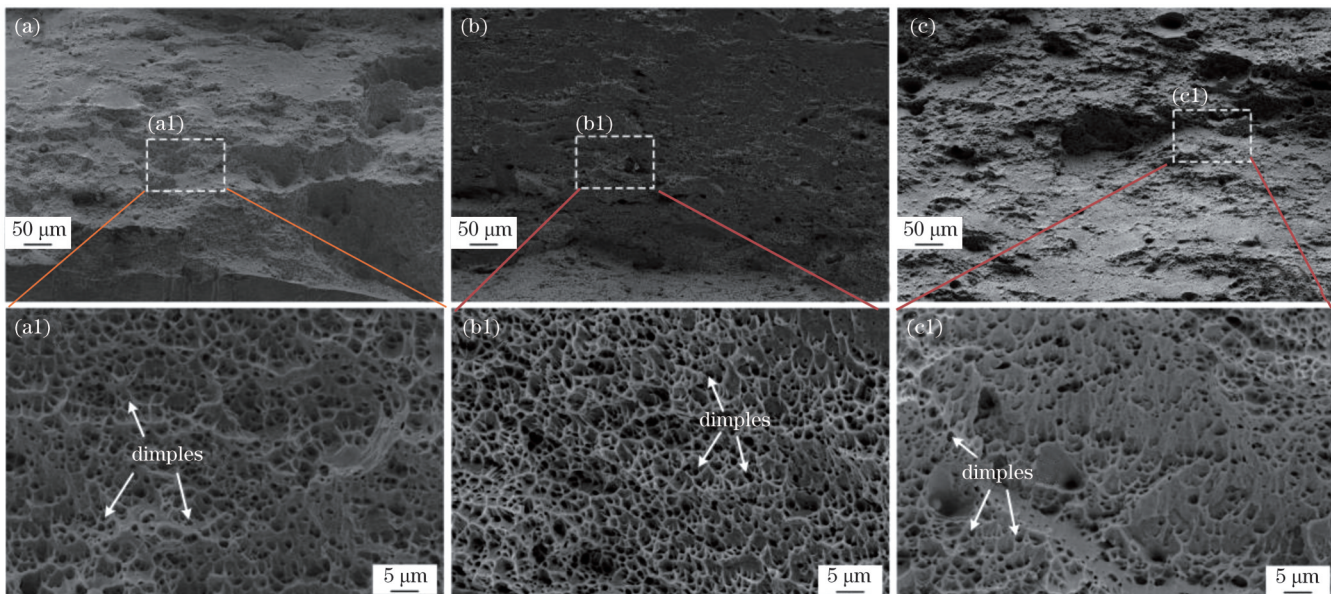


图 10 不同热输入下的断口形貌。(a)低热输入($90 J/mm$);(b)中热输入($150 J/mm$);(c)高热输入($200 J/mm$)

Fig. 10 Fracture morphologies under different heat inputs. (a) Low heat input ($90 J/mm$); (b) medium heat input ($150 J/mm$); (c) high heat input ($200 J/mm$)

塑性较好,断面收缩率也较高。在低热输入($90 J/mm$)条件下获得的接头的断口表面存在着尺寸较大且较深的等轴韧窝;随着热输入的增加,等轴韧窝的尺寸和深度逐渐减小。

4 结 论

在低热输入($90 J/mm$)条件下,焊缝中的柱状晶粒由于冷却速度快而生长受限,因此晶粒尺寸相对较小。而在高热输入($200 J/mm$)条件下,熔池中 Marangoni 对流流动导致焊缝横截面呈现 X 形状,并引起横截面尺寸明显增加,同时液态熔池经历的最高温度增加,导致晶界的迁移和晶粒的粗化,因此柱状晶晶粒的尺寸增大。

随着焊接热输入的增加,在焊缝中心线附近出现了少量的细小等轴亚晶结构。相比于高热输入,低热输入下晶粒的竞争生长程度相对较弱,焊缝的平均晶

粒面积细化了 29.8%;同时焊缝底部等轴亚晶粒的数量增多,尺寸减小,焊缝中心线附近的平均二次枝晶间距仅为 $5.12 \mu m$ 左右,相较于高热输入下的减少了 $0.99 \mu m$ 。

焊缝中晶粒的形态和尺寸会影响焊接接头局部区域的应力-应变分布,从而影响接头的强度和塑性,因此接头的抗拉强度由 473.4 MPa 降低至 432.9 MPa ,延伸率从 20.7% 下降至 15.3% ,断裂位置均位于焊缝区域。在低热输入下获得的接头的断口表面存在着尺寸较大且较深的等轴韧窝,并且随着热输入的增加,等轴韧窝的尺寸和深度逐渐减小。

参 考 文 献

- [1] 黄钢华, 张冬梅, 晏冬秀, 等. Invar 钢模具制造工艺研究[J]. 航空工程进展, 2011, 2(4): 485-488.
Huang G H, Zhang D M, Yan D X, et al. Manufacturing technology research on invar steel mould[J]. Advances in

- Aeronautical Science and Engineering, 2011, 2(4): 485-488.
- [2] Soutis C. Fibre reinforced composites in aircraft construction[J]. Progress in Aerospace Sciences, 2005, 41(2): 143-151.
- [3] Lagarec K, Rancourt D G, Bose S K, et al. Observation of a composition-controlled high-moment/low-moment transition in the face centered cubic Fe-Ni system: Invar effect is an expansion, not a contraction[J]. Journal of Magnetism and Magnetic Materials, 2001, 236(1/2): 107-130.
- [4] 刘扬. 民机 Invar 模具钢 MIG 自动焊接工艺研究[D]. 南京: 南京航空航天大学, 2015.
- Liu Y. Study on MIG automatic welding technology of civil aircraft Invar die steel[D]. Nanjing: Nanjing University of Aeronautics and Astronautics, 2015.
- [5] 凌万里. Invar 合金模具典型结构焊接参数化建模与工艺优化研究[D]. 南京: 南京航空航天大学, 2020.
- Ling W L. Study on welding parametric modeling and process optimization of typical structure of Invar alloy mold[D]. Nanjing: Nanjing University of Aeronautics and Astronautics, 2020.
- [6] Wang Q, Dong Y W, Jiang Z H, et al. Enhancing low thermal expansion behavior and strength via induced Zr-rich intermetallic phase in Fe-36Ni Invar alloy[J]. Materials & Design, 2023, 226: 111644.
- [7] Jiao G H, Fang X W, Chen X M, et al. The origin of low thermal expansion coefficient and enhanced tensile properties of Invar alloy fabricated by directed energy deposition[J]. Journal of Materials Processing Technology, 2023, 317: 117994.
- [8] Rao X X, Ru Y D, Guo F M, et al. Abnormal strain evolution of austenite upon martensitic transformation in FeNiCo alloy with invar effect: an *in situ* study[J]. Scripta Materialia, 2022, 220: 114942.
- [9] 吴东江, 张天武, 马广义, 等. 连续激光焊接 Fe-Ni 合金工艺参数对焊缝形貌的影响[J]. 中国激光, 2013, 40(3): 0303003.
- Wu D J, Zhang T W, Ma G Y, et al. Influence of welding parameters on the morphology of Fe-Ni alloy with continuous wave YAG laser[J]. Chinese Journal of Lasers, 2013, 40(3): 0303003.
- [10] 吴东江, 尹波, 张维哲, 等. Nd:YAG 激光焊接殷钢材料的工艺研究[J]. 中国激光, 2008, 35(11): 1773-1777.
- Wu D J, Yin B, Zhang W Z, et al. Nd:YAG laserbeam welding Invar 36 alloy[J]. Chinese Journal of Lasers, 2008, 35(11): 1773-1777.
- [11] Li G, Gao M, Chen C, et al. Characterisation comparison of laser and laser - arc hybrid welding of Invar 36 alloy[J]. Science and Technology of Welding and Joining, 2014, 19(1): 30-37.
- [12] Zhao J Y, Wang J Y, Kang X F, et al. Effect of beam oscillation and oscillating frequency induced heat accumulation on microstructure and mechanical property in laser welding of Invar alloy[J]. Optics & Laser Technology, 2023, 158: 108831.
- [13] Li Y F, Wang F, Liu H B, et al. Effect of surface roughness on the performances of laser-welded Invar 36 alloy joints[J]. Optics & Laser Technology, 2023, 162: 109307.
- [14] 刘红兵, 宣扬, 杨瑾. Invar 合金焊接技术研究现状及展望[J]. 航空制造技术, 2020, 63(9): 83-88, 102.
- Liu H B, Xuan Y, Yang J. Research status and prospect of invar alloy welding technology[J]. Aeronautical Manufacturing Technology, 2020, 63(9): 83-88, 102.
- [15] 程昊, 周炼刚, 刘健, 等. 热输入对 Inconel 617 镍基高温合金激光焊接接头显微组织与力学性能的影响[J]. 材料工程, 2023, 51(1): 113-121.
- Cheng H, Zhou L G, Liu J, et al. Effect of heat input on microstructure and mechanical properties of laser welded joint of Inconel 617 nickel-based superalloy[J]. Journal of Materials Engineering, 2023, 51(1): 113-121.
- [16] 张天武. 激光焊接工艺对 Fe-Ni 合金焊缝质量的影响[D]. 大连: 大连理工大学, 2013.
- Zhang T W. Effect of laser welding process on weld quality of Fe-Ni alloy[D]. Dalian: Dalian University of Technology, 2013.
- [17] StJohn D H, Prasad A, Easton M A, et al. The contribution of constitutional supercooling to nucleation and grain formation[J]. Metallurgical and Materials Transactions A, 2015, 46(11): 4868-4885.
- [18] Jiang Z G, Chen X, Li H, et al. Grain refinement and laser energy distribution during laser oscillating welding of Invar alloy[J]. Materials & Design, 2020, 186: 108195.
- [19] Hao K D, Gong M C, Pi Y M, et al. Effect of Ni content on rolling toughness of laser-arc hybrid welded martensitic stainless steel[J]. Journal of Materials Processing Technology, 2018, 251: 127-137.
- [20] Cui S W, Shi Y H, Sun K, et al. Microstructure evolution and mechanical properties of keyhole deep penetration TIG welds of S32101 duplex stainless steel[J]. Materials Science and Engineering: A, 2018, 709: 214-222.
- [21] 陈丹, 刘婷, 赵艳秋, 等. 晶粒尺寸对双激光束双侧同步焊接接头力学性能的影响[J]. 中国激光, 2021, 48(10): 1002120.
- Chen D, Liu T, Zhao Y Q, et al. Effect of grain size on mechanical properties of double laser-beam bilateral synchronous welding joint [J]. Chinese Journal of Lasers, 2021, 48(10): 1002120.
- [22] 方辉, 薛桦, 汤倩玉, 等. 定向凝固糊状区枝晶粗化和二次臂迁移的实验和模拟[J]. 金属学报, 2019, 55(5): 664-672.
- Fang H, Xue H, Tang Q Y, et al. Dendrite coarsening and secondary arm migration in the mushy zone during directional solidification: experiment and simulation[J]. Acta Metallurgica Sinica, 2019, 55(5): 664-672.
- [23] Ren W J, Lu F G, Yang R J, et al. A comparative study on fiber laser and CO₂ laser welding of Inconel 617[J]. Materials & Design, 2015, 76: 207-214.

Research on Microstructure Evolution and Tensile Properties of Laser Welded Joints of Domestic Invar Alloy

Zhou Yuqi¹, Chen Lihong¹, Wang Jianfeng¹, Li Zhu², Mu Zhan², Zhan Xiaohong^{1*}

¹College of Materials Science and Technology, Nanjing University of Aeronautics and Astronautics, Nanjing 211106, Jiangsu, China;

²Xi'an Gangyan Special Alloy Co., Ltd., Xi'an 710000, Shaanxi, China

Abstract

Objective Since the discovery of the Invar alloy by foreign scientists in the 19th century, it has been of great importance because of its extremely low coefficient of thermal expansion, which is very similar to that of composite materials. It is thus widely used as an important material for large-scale composite dies in the aerospace field. In the domestic development of Invar alloys, their thermal, physical, and mechanical properties have been the main focus of attention; however, only a few scholars have studied the welding

process of domestic Invar alloys and reported results have been limited to process parameters and other aspects. Therefore, this study contrastively analyzes the microstructural differences of welded joints of 4 mm thick domestic Invar alloy obtained under different laser heat inputs and studies the effects of grain morphology, texture, and grain size in the weld seam on the tensile properties of the welded joints.

Methods The dimensions of the welded parts used in this experiment are 100 mm×50 mm×4 mm (Fig. 1). A fiber laser is used as the laser source in this experiment. After passing through the collimator and focusing mirror, the laser spot on the surface of the plate has a diameter of 0.3 mm. Scanning electron microscopy (SEM) is used to observe the microstructure of the joint cross section and the tensile fracture morphology according to the obtained tissue morphology to study the microstructural characteristics of the joints under different heat inputs. Electron backscatter diffraction (EBSD) technology is used to observe the grain size and orientation of the weld seams.

Results and Discussions The laser welded joint is divided into three zones: weld fusion zone, base metal, and narrow heat-affected zone. There is an obvious boundary of the grain growth intersection at the center of the weld seam. As the welding heat input increases, the size of the weld cross section significantly increases (Figs. 3 and 4). The weld seam is mainly composed of large columnar grains, and primary and secondary dendrites are clearly observed near the centerline of the weld seam (Fig. 5). The metal solidification of an Invar alloy laser-welded joint is a rapid and directional solidification process that involves epitaxial growth on the base metal. The ratio of the temperature gradient to the cooling rate determines the degree of component undercooling, which has a significant impact on the dendritic morphology of the solidified structure (Fig. 6). The grain orientation in the middle of the weld seam under a high heat input is relatively disordered and the texture strength is high, indicating that the grain competition growth mechanism is stronger than that under a low heat input. Meanwhile, the average grain area under a low heat input is refined by 29.8% compared with that under a high heat input (Fig. 7). Compared to those under the high heat input, the number of sub-grains at the bottom of the weld seam increases and their size decreases under the low heat input, with an average secondary dendrite spacing of approximately 6.11 μm decreasing to approximately 4.26 μm (Fig. 8). The tensile results indicate that the grain coarsening caused by increased heat input leads to a decrease in the tensile strength of welded joint from 473.4 MPa to 432.9 MPa, while the size and depth of equiaxed dimples at the fracture surface are significantly reduced (Figs. 9 and 10).

Conclusions The microstructural differences of welded joints of 4 mm thick domestic Invar alloy obtained under different laser heat inputs are contrastively analyzed, and the effect of grain size on the tensile properties of welded joints is studied. The results show that the weld seam is primarily composed of columnar dendrites, and the grain growth mode is similar under different heat inputs. However, the size of the columnar grains gradually increases with increasing heat input. The average grain area under the low-heat-input (90 J/mm) condition is 12599.7 μm², refined by 29.8% compared to that under the high heat input (200 J/mm), and the number of sub-grains at the bottom of the weld seam increases and the size decreases under the low heat input, with an average secondary dendrite spacing of approximately 6.11 μm decreasing to approximately 4.26 μm. The tensile results indicate that the grain coarsening caused by increased heat input leads to a decrease in the tensile strength of the welded joint from 473.4 MPa to 432.9 MPa, while the size and depth of equiaxed dimples at the fracture surface are significantly reduced.

The growth of columnar grains in the weld seam is limited due to the fast-cooling rate under the low heat input (90 J/mm), resulting in relatively small grain sizes. Under the high heat input (200 J/mm), due to the Marangoni convective flow in the molten pool, the weld cross section presents an X-shaped shape and causes a significant increase in cross-sectional size. At the same time, the highest temperature experienced by the liquid molten pool gradually increases, leading to grain boundary migration and grain coarsening, resulting in a gradual increase in the size of columnar grain.

With an increase in welding heat input, a small amount of fine equiaxed sub-grain structure appears near the centerline of the weld seam. Compared to that under the high heat input, the competitive growth degree of grains under the low heat input is relatively weak, and the average grain area of the weld seam has also been refined by 29.8%. At the same time, the number of equiaxed sub-grain structures at the bottom of weld seam increases, the size decreases, and the average secondary dendrite spacing near the centerline of the weld is only about 5.12 μm, which is 0.99 μm less than that under high heat input.

The morphology and size of grains can affect the stress-strain distribution in local areas of the welded joint, thereby affecting the strength and plasticity of the welded joint. The tensile strength of the welded joint decreases from 473.4 MPa to 432.9 MPa, and the elongation decreases from 20.7% to 15.3%. The fracture morphology of the welded joint indicates that the size and depth of equiaxed dimples gradually decrease with increasing heat input.

Key words laser technique; laser welding; domestic Invar alloy; microstructure evolution; grain size; tensile property